Chapter 6
MRI Assessment of the Tricuspid Valve and Right Heart

Vien T. Truong, Cassady Palmer, Justin T. Tretter, Tarek Alsaied, Michael D. Taylor, and Wojciech Mazur

Introduction

Although there have been improvements in cardiac imaging, assessing the complex geometries of the right atrium (RA), tricuspid valve (TV), and right ventricle (RV) remains a challenge with strictly two-dimensional imaging. The substernal (anterior) position and complex morphology of these structures underlie much of this difficulty [1].

Transthoracic echocardiography, radionuclide ventriculography, and computed tomography are commonly used in clinical practice to qualitatively monitor RV size and systolic function. Given the complex shape, thin wall, and substernal location of the RV, echocardiography evaluation is limited. Computed tomography can circumnavigate some of these, though it exposes patients to ionizing radiation. CMR provides the most comprehensive evaluation of the RV. It is the gold standard for quantification of ventricular volume and ejection fraction with additional benefits of tissue characterization and accurate quantification of blood flow [2, 3]. CMR affords a reasonable compromise of high temporal, spatial, and contrast

V. T. Truong
The Christ Hospital Health Network, Cincinnati, OH, USA

The Lindner Research Center, Cincinnati, OH, USA

C. Palmer · W. Mazur (✉)
The Christ Hospital Health Network, Cincinnati, OH, USA
e-mail: wojciech.mazur@thechristhospital.com

J. T. Tretter · M. D. Taylor
The Heart Institute, Cincinnati Children's Hospital Medical Center, University of Cincinnati College of Medicine, Cincinnati, OH, USA

T. Alsaied
The Heart Institute, UPMC Children's Hospital of Pittsburgh, University of Pittsburgh School of Medicine, Pittsburgh, PA, USA

© Springer Nature Switzerland AG 2022

H. Mathelier et al. (eds.), *Tricuspid Valve Disease*, Contemporary Cardiology,
https://doi.org/10.1007/978-3-030-92046-3_6

resolution with a wide field of view without radiation exposure. The interest in CMR is based on these features, as well as the reproducible nature of volumetric and flow measurements [2, 4]. The RV and TV can be evaluated from multiple planes using steady-state free precession (SSFP) sequences. SSFP techniques have been validated for the quantification of ventricular volumes and function and evaluating valvular structures [5]. Gradient echo (GRE) imaging allows for accurate visualization of stenotic and regurgitant flow [5]. Furthermore, quantification of flow across the TV and pulmonary valve can be evaluated using phase-contrast velocity-encoding [5]. RV systolic function is most commonly assessed by global metrics (e.g., ejection fraction, stroke volume, cavity volume, and myocardial thickness); however, regional assessment can also be obtained [3]. Recent research has shown regional changes in strain and strain rate were sensitive for detecting early manifestations of dysfunction and so may provide additional information when assessing RV systolic function [6, 7].

This chapter will provide a brief synopsis of the underlying principles of CMR assessment as it relates to RV function and the TV.

CMR Pulse Sequences and Strain: General Principles

There are a variety of CMR pulse sequences used in cardiac imaging. The most common pulse sequences for the assessment of ventricular function and heart valvular disease are summarized in Table 6.1 [8] and discussed in this section.

Table 6.1 CMR pulse sequences with utility in the evaluation of valvular heart disease

CMR pulse sequence	Utility
Steady-state free precession cine	Valve anatomy and leaflet motion Ventricular volumes and function Turbulent blood flow jet visualization
Gradient echo cine	Valve anatomy and leaflet motion Turbulent blood flow jet visualization Prosthetic valve assessment
Phase contrast	Flow velocity Forward and regurgitant volumes
Turbo spin echo	Evaluation of valve masses
Segmented inversion recovery gradient echo	Evaluation of valve masses

Adapted from Gulsin et al. [8]. This article is distributed under the terms of the Creative Commons Attribution 4.0 International License (http://creativecommons.org/licenses/by/4.0/)

Steady-State Free Precession

Steady-state free precession (SSFP) sequences are gradient echo sequences with a short repetition time in which a steady residual transverse magnetization is maintained between successive cycles [9]. SSFP provides a high signal-to-noise ratio and excellent contrast between the blood pool and myocardium. RV volumes are measured from the plane of the TV to the RV apex using either axial or short-axis stacks [10]. Endocardial and epicardial contours are drawn at both end-diastolic and end-systolic phases of the cardiac cycle throughout the stack, allowing for accurate calculation of RV volumes, ejection fraction, and myocardial mass (Fig. 6.1). Although there are advantages of SSFP imaging, among the limitations is the possibility of signal loss. Marked signal loss can occur in regions of flow turbulence or susceptibility artifacts due to magnetic field inhomogeneities. To minimize any signal loss, echo times for SSFP imaging are kept relatively short. Furthermore, it is imperative to properly align planes when more than one jet is present in order to identify the mechanism of regurgitation and the location of the regurgitant jets.

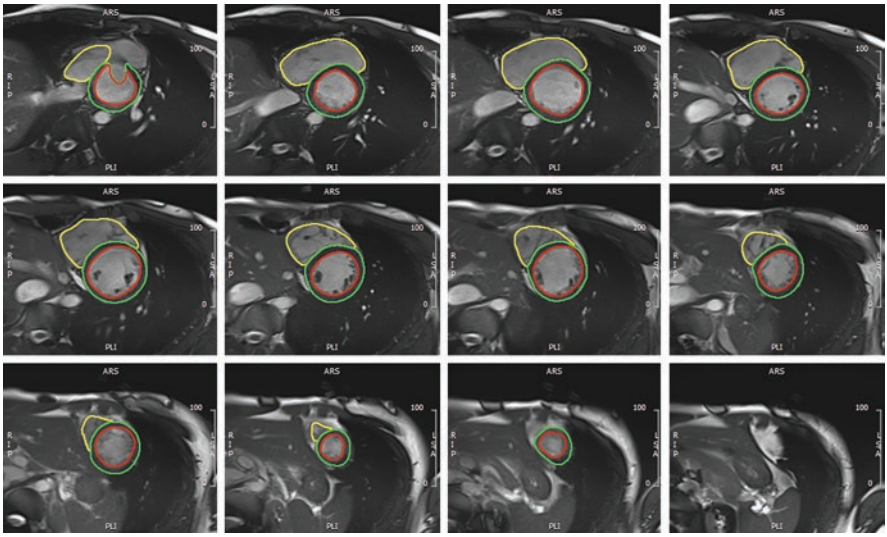

Fig. 6.1 Steady-state free precession sequence in short-axis view. RV volume, ejection fraction, and mass are calculated using an SSFP short-axis stack. Endocardial and epicardial contours are drawn at both end-diastole and end-systole throughout the stack. SSFP steady-state free precession sequence

GRE Imaging

GRE imaging uses increased spin dephasing, which improves the sensitivity of detecting abnormal flow, and is less subject to signal loss compared to SSFP imaging. GRE short-axis stacks can be used to measure valve orifice area. This can be performed by using slightly overlapped slices while giving attention to ensure there is complete visualization through the orifice. This technique is more accurate when the orifice has a simple shape, and the jet is coherent. Irregular regurgitant jet shapes with multiple components compromise the sensitivity of this technique.

Phase Contrast Mapping

Phase-contrast velocity mapping utilizes gradient velocity-encoding to generate a phase shift of moving protons within the magnetic field [11]. Velocity mapping imaging can be used to measure jet velocity and volume flow. The intensity of the phase images is directly proportional to the velocity of spins within each voxel, which allows for quantitative assessment of flow velocities. Directional components (*X*, *Y*, and *Z* planes) of velocity are encoded; however, the through plane (slice selection) is assigned to the *Z*-plane. Phase-contrast velocity mapping is susceptible to aliasing, which occurs when the maximum measurable encoding velocity (V_{ENC}) is set too low. In contrast, when the V_{ENC} is set too high, sensitivity is reduced. The optimal V_{ENC} is ~10% greater than the maximum velocity component in the image.

CMR-Derived Strain

Strain is defined as the deformation of an object in response to an applied force and is conventionally reported as a percent change. The speed at which the deformation occurs is termed as strain rate. Regional strain can be calculated using the Lagrangian formula: $[e = (L - Lo)/Lo]$, where e is strain, Lo is original length, and L is the length of the object after the applied force resulting in deformation. A negative strain value occurs when L is shorter than Lo, and a positive strain value occurs when L exceeds Lo. Strain is a tensor and can be calculated in three principal directions (longitudinal, circumferential, and radial). There are several CMR acquisition techniques that can be used to analyze strain, including myocardial tagging, displacement-encoding (DENSE), strain encoding (SENC), and feature tracking (FT) [12]. While myocardial tagging MRI is the gold standard for myocardial deformation, this method is time-consuming. This spurred the development of FT-CMR, which is less time-consuming (Fig. 6.2), and analogous to speckle-tracking echocardiography. FT-CMR is a post-processing technique in which myocardial tissue signatures in cine images are tracked to measure heart deformation. Endocardial

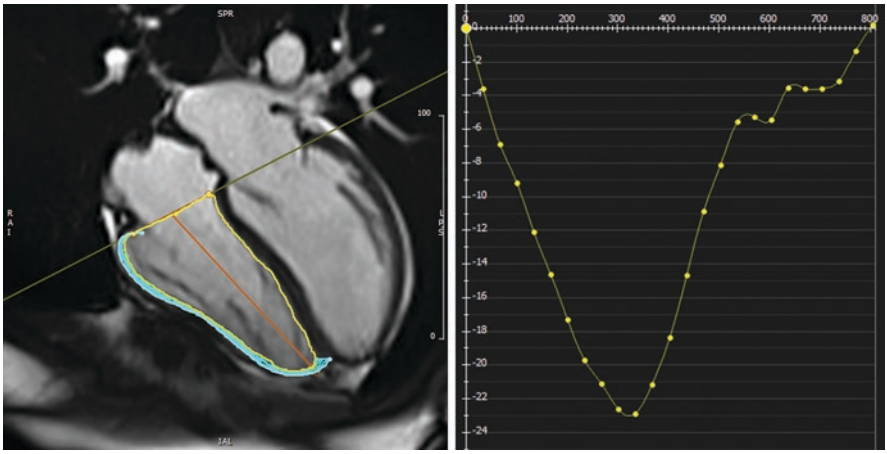

Fig. 6.2 Cardiovascular magnetic resonance-tissue tracking in the assessment of right ventricular function. Longitudinal strain in the apical four-chamber view with the strain curve demonstrated

and epicardial borders are delineated and tracked using cine imaging from short-axis and three long-axis views (four-chamber, two-chamber, and three-chamber) throughout the cardiac cycle. FT-CMR has good intra- and inter-observer reproducibility [13–15]. An important advantage is that it can be applied to SSFP imaging, which is commonly part of routine CMR protocols, thus requiring no additional sequences.

CMR Assessment in Tricuspid Valve and Right Heart Disease

Right Atrium Anatomy, Size, and Function

The RA is less uniform in thickness compared to the left atrium. The terminal crest demarcates the junction between the right atrial appendage and venous inflow. Pectinate muscles arise from the terminal crest and course in branched and often overlapping fashion toward the TV. The prominent RA musculature underlies the increased TV ring excursion compared to the mitral valve [16]. Atrial size and function, including atrial strain, can be measured by CMR. CMR offers advantages compared to echocardiography for evaluating the RA: wider field of view, greater signal-to-noise ratio with improved image quality, and border tracking for the RA [17]. Normal values for right atrial function are provided in Table 6.2. Similar to the assessment of ventricular deformation, the quantitative assessment of atrial deformation by feature tracking or tissue tracking is reproducible [18]. Regional deformation for both atria can be compared to measure inter-atrial dyssynchrony. In addition, assessment for late gadolinium enhancement as a measure of atrial wall

Table 6.2 Ventricular reference range for Caucasian adults

Parameters	Men	Women
RV EDV (ml)	124–248	85–168
RV ESV (ml)	47–123	27–77
RV SV (ml)	62–131	48–99
Indexed RV EDV (ml/m^2)	68–125	53–99
Indexed RV ESV (ml/m^2)	25–63	17–46
Indexed RV SV (ml/m^2)	34–67	30–59
RV EF (%)	45–65	47–68
Maximal RA volume (ml)	43–143	38–101
RA SV (ml)	10–66	14–52
Indexed maximal RA volume (ml)	22–74	23–59
Indexed RA SV (ml/m^2)	5–33	8–31
RA EF (%)	23–58	31–63
RV longitudinal strain (%)[a]	−19.71 to −22.73	−19.71 to −22.73
RV circumferential strain (%)[a]	−10.35 to −12.02	−11.14 to −13.04

EDV end-diastolic volume, *EF* ejection fraction, *ESV* end-systolic volume, *RA* right atrium, *RV* right ventricle, *SV* stroke volume. The normal ranges were defined as the range where the measured value fell within the 95% prediction interval

[a]Reprinted from Truong et al. [15]. Copyright 2017, with permission from Elsevier. Adapted from Ref. [81]

fibrosis is possible by CMR, although improved sequences with very good spatial resolution are required for this to be adopted widely in clinical practice due to the thin atrial wall [19].

Tricuspid Valve Anatomy and Function

When viewed using standard orthogonal body coordinates, the TV consists of the anterosuperior (often referred to as anterior), septal, and inferior (often referred to as posterior) leaflets [20]. For purposes of concordance with clinical literature, we will refer to the anterosuperior leaflet as "anterior" and inferior leaflet as "posterior." The TV is the largest cardiac valve with a wide variability in the number and morphology of the leaflets [1, 21]. Compared to the mitral valve, the TV annulus is located slightly closer to the apex and has papillary muscle and direct chordal attachments to the interventricular septum. One of the most consistent features of the TV and its supporting apparatus are the multiple direct chordal attachments tethering the septal leaflet to the interventricular septum (Fig. 6.3). In contrast, there is marked variability in the morphology and location of the supporting papillary muscles. The anterior and septal leaflets are usually the largest, and the posterior leaflets are generally the smallest of the three [1]. The normal tricuspid annulus is a complex nonplanar structure, measuring approximately 4–6 cm^2 in area in adults when fully open in diastole, with dynamic changes throughout the cardiac cycle and under varying loading conditions [22].

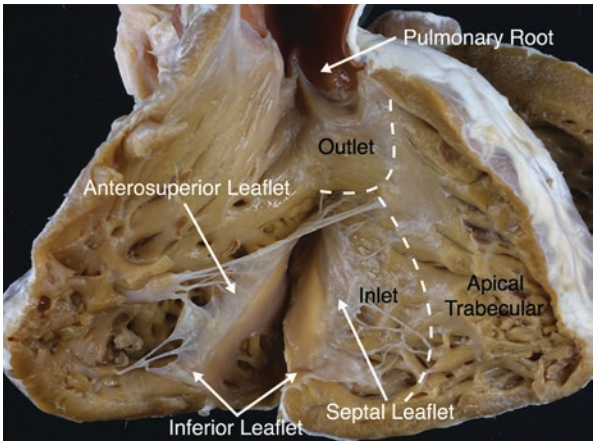

Fig. 6.3 Normal right ventricle and tricuspid valve. This normal heart specimen is opened to view the right ventricular cavity and tricuspid valve. The three leaflets of the tricuspid valve are visualized (anterior, septal, and posterior leaflets) guarding the inlet of the right ventricle. The tripartite right ventricle consists of inlet, apical trabecular, and outlet components with the hashed white lines marking the boundaries between each

CMR evaluation of TV leaflet morphology can be challenging because the normal leaflets are thin. Thin slice SSFP cine imaging is used to assess the anatomy and function of the TV. Common imaging planes include the four-chamber cine to assess the anterior and septal leaflets and the RV inflow or two-chamber and RV inflow/outflow cines, which can assess the anterior and posterior leaflets (Fig. 6.4). The short-axis cine stack slices through the TV en face. Conventional and time-resolved magnetic angiography allows for multiplanar reformatting and 3D CMR reconstruction, which can provide a detailed anatomical evaluation of the TV [23–25].

Right Ventricle Anatomy, Size, and Function

The normal RV is tripartite with an inlet, apical trabecular, and outlet component (see Fig. 6.4). The inlet of the RV extends from the TV annular plane to its chordal and papillary muscle attachments on the interventricular septum and RV free wall. The apical trabecular component has coarse trabeculations with the prominent and distinct moderator band coursing from the septum to RV free wall [26] (see Fig. 6.3). The normal RV outlet differs from the left ventricular outlet. In the RV, there is a free-standing muscular sleeve or infundibulum that lifts the pulmonary root away from the base of the heart resulting in fibrous discontinuity between the TV and pulmonary valve [27]. By two-dimensional imaging, the RV appears crescent shaped when viewed in its short axis and pyramidal shaped in its long axis.

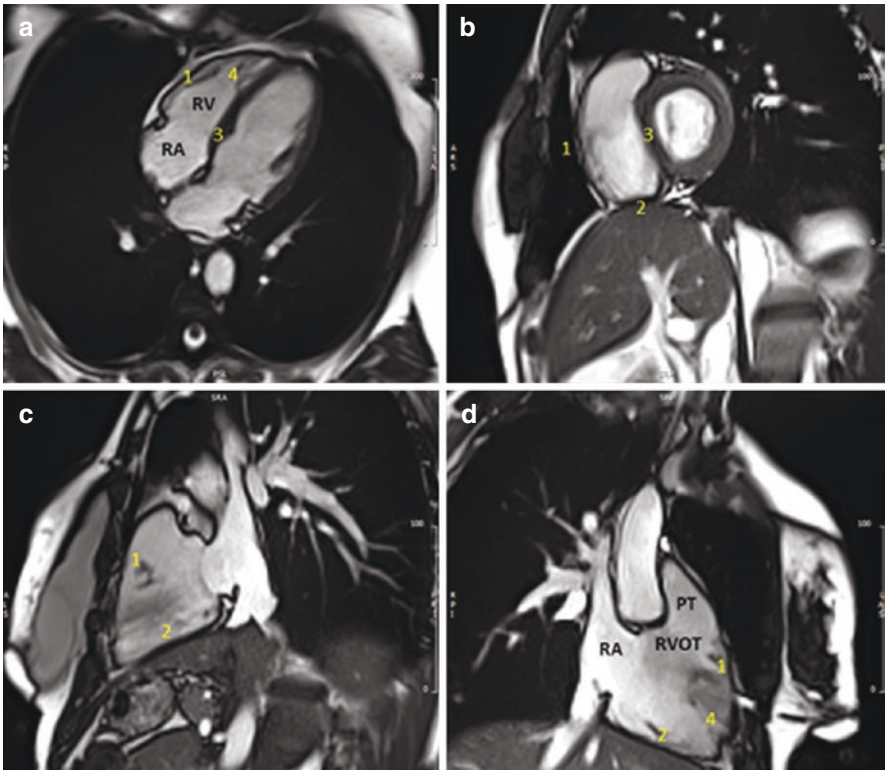

Fig. 6.4 Cardiovascular magnetic resonance in the assessment of right ventricle and tricuspid valve. (**a**) Four-chamber view: evaluates the inflow and the apical trabecular portion of the RV, the septal and anterior leaflets of the tricuspid valve; (**b**) Short-axis view: a stack can be obtained through the entire tripartite RV, viewing the three leaflets of the tricuspid valve en face at the base of the heart; (**c**) RV inflow: evaluates the inflow and the apical trabecular portion of the RV, and the anterior and posterior leaflets of the tricuspid valve; (**d**) RV inflow/outflow: evaluates the entire tripartite RV from the inlet to apical trabecular to outlet components, viewing the anterior and posterior leaflets of the tricuspid valve. RV right ventricle, TR tricuspid valve, RA right atrium, PT pulmonary trunk, RVOT right ventricular outflow tract; (1), anterior wall; (2), inferior wall; (3), interventricular septum; (4), trabecular bands

Contraction of the RV consists of a peristalsis-like motion with synchronized contraction occurring from the inlet and apex toward the outlet [28]. This predominately longitudinal shortening with delay in contraction from inlet to outlet of approximately 20–50 ms results in indistinct isovolumetric periods, in contrast to the left ventricular contraction pattern [28, 29]. The end-diastolic volume of the normal RV is on average 10–15% larger than that of the LV, with approximately 20% of its volume accounted for by the infundibulum. The RV free wall is thinner than that of the LV and is one-sixth to one-third the mass of the LV [28].

There are several methods used to measure RV systolic function, including volumetric and tissue tracking techniques. Ventricular systolic function can be estimated

by measuring the ejection fraction by CMR using the Simpson method. This method uses a stack of contiguous slices of the entire ventricle. The ventricular volume is the sum of the individual slice volumes (slice thickness × slice area). The RV stroke volume (SV) can be noninvasively calculated as the difference of end-diastolic volume (EDV) and end-systolic volume (ESV) (SV = EDV − ESV). The ejection fraction is the SV divided by EDV (SV/EDV). Normal reference values for RV function using CMR are provided in Table 6.2.

Right Atrial Pathology

Right Atrial Dysfunction

Right atrial dysfunction is now recognized as a distinct clinical entity [30]. RA dysfunction is important in pulmonary arterial hypertension, heart failure, and CHD. It has been shown to be a predictor of clinical outcomes in a variety of cardiovascular diseases [31–34]. CMR is the gold standard modality for the assessment of the RA function due to its excellent spatial resolution and endocardial border definition. CMR-derived RA strain allows identification of all phases of RA dynamics (reservoir, conduit, and booster function) [35], allowing for detection of subclinical dysfunction [36]. Whether or not RA function will be relevant to the success of individualized TV interventions remains to be determined.

Tricuspid Valve Pathology

Tricuspid Valve Regurgitation

Physiological TR, often termed trivial, is a common finding in healthy individuals, while pathological TR is commonly a consequence of annular dilation, increased RV pressure, or a leaflet abnormality. Left-sided heart failure resulting in RV hypertension is the most common cause of TR in adults. There are multiple congenital TV malformations, including leaflet dysplasia, annular hypoplasia, leaflet cleft, Ebstein anomaly, and leaflet prolapse. Annular dilation of the TV with resulting functional TR as a result of RV dilation is also common in many forms of congenital heart disease (CHD), such as repaired tetralogy of Fallot.

Velocity encoding can be used to directly quantify TR from a short-axis en face acquisition (Fig. 6.5). However, this technique is challenging due to the movement of tricuspid annulus. Dephasing allows for planimetry of a clearly delineated vena contracta, and >7 mm suggests the presence of severe TR [37]. There are quantitative techniques that allow for indirect quantification of TR. RV stroke volume (SV) can be compared to the pulmonary valve forward flow and can be used to calculate

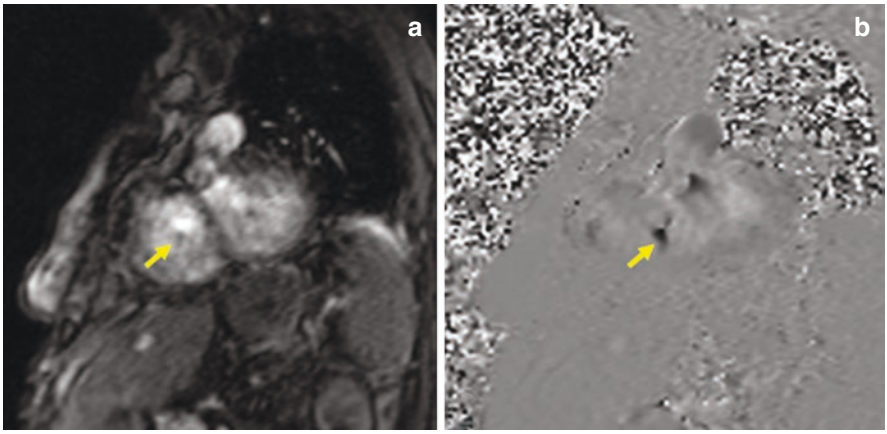

Fig. 6.5 Tricuspid regurgitation on gradient recalled echo and phase-contrast velocity imaging. (**a**) Gradient recalled echo imaging demonstrating non-coaptation of the tricuspid valve (yellow arrow); (**b**) phase-contrast velocity encoded imaging demonstrating tricuspid valve regurgitation (yellow arrow) at the level of valve orifice in short-axis view

TR: TR fraction = (RV SV − pulmonary valve forward flow)/RV SV × 100%. It should be noted that this technique is susceptible to error in any situation where there is significant intracardiac shunting, beat-to-beat variability of SV, such as an arrhythmia or significant pericardial effusion, since the RV stroke volume and pulmonary valve phase-contrast sequences are acquired over multiple heartbeats. Alternatively, ventricular SVs can be compared (RV SV − left ventricular SV)/RV SV × 100% [25]. This technique becomes difficult to use in the setting of polyvalvular regurgitation and also becomes less reliable in the face of arrhythmia. Finally, in the absence of significant atrial level shunting, the TR regurgitant fraction can be calculated using tricuspid and mitral valve antegrade diastolic flow using the following formula: TR regurgitant flow = TV diastolic flow – mitral valve diastolic inflow. This technique becomes less useful if there is mitral regurgitation.

CMR in Transcatheter Tricuspid Valve Interventions

Severe TR is associated with poor prognosis if left untreated. The current recommendations for TR intervention include (1) severe TR undergoing left-sided valve surgery, (2) mild or moderate functional TR at the time of left-sided valve surgery with tricuspid annular dilation or evidence of right heart failure, and (3) severe primary TR with symptoms unresponsive to medical therapy [38, 39]. The recent guidelines emphasize the importance of early treatment of TR [38]. Though still in clinical trials, transcatheter interventions have emerged as alternatives to conventional surgery in the management of TV disease because of the growing number of

high surgical risk elderly patients [25]. Recently, 6-month outcomes have suggested the safety of the transcatheter interventions in patients with symptomatic and moderate to severe functional TR with a decrease of annular dimensions, a significant reduction in regurgitant severity, improvements in heart failure symptoms, improved quality of life, and increased exercise capacity [40]. The primary imaging modality for diagnosis and longitudinal evaluation of tricuspid regurgitation is two-dimensional echocardiography with supplemental three-dimensional echocardiography; however, CMR imaging can be used to inform the timing of TV surgery and assess potential hemodynamic improvements after intervention [25, 41].

Tricuspid Valve Stenosis

Tricuspid stenosis is decreasing in incidence and, when diagnosed, is commonly attributed to rheumatic heart disease [38, 42]. Other causes include infective endocarditis, carcinoid, endomyocardial fibrosis, systemic lupus erythematous, and congenital TV lesions [42]. Varying degrees of TV hypoplasia and resulting stenosis are also seen in forms of congenital heart disease (CHD), such as pulmonary atresia with an intact ventricular septum.

CMR use in the setting of tricuspid stenosis has not been well studied. However, tricuspid stenosis by CMR will typically demonstrate thickened leaflets with restricted excursion during diastole [42, 43]. Tricuspid stenosis is often visualized as a signal void during the diastolic phase extending into the RV. CMR short-axis images and phase velocity maps can be aligned to transect the stenotic lesion close to the orifice. A valve orifice measured in diastole from short-axis images of <1 cm^2 is indicative of severe stenosis [42].

Right Ventricle Pathology

Ischemic Heart Disease

RV infarction has been reported in as many as 50% of cases involving inferior myocardial infarctions and 33% of all anterior myocardial infarctions [44–46]. RV systolic dysfunction resulting from concomitant left ventricular myocardial infarction is associated with higher rates of morbidity and mortality [47]. The RV ejection fraction and degree of regional wall motion abnormalities are important prognostic markers. RV infarction can be detected and evaluated by the use of late gadolinium enhancement (LGE) (Fig. 6.6) and T2-weighted imaging. Tissue characterization assessing myocardial edema and detection of LGE help differentiate reversible and irreversible injury.

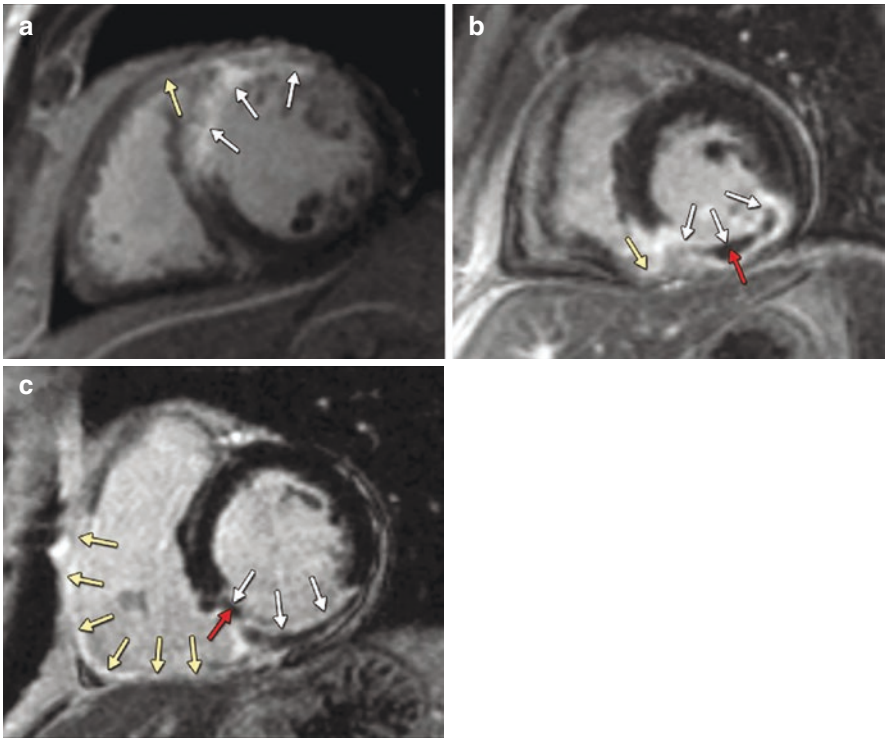

Fig. 6.6 Right ventricular myocardial infarction on late enhancement cardiovascular magnetic resonance imaging. (**a**) LGE is present in the anterior part of the RV free wall in a patient with anterior STEMI; (**b**, **c**) LGE is present in the inferior or both the inferior and the mid-part of RV free wall in patients with inferior STEMI. Yellow arrows indicate LGE in RV free wall, white arrows indicate LGE in left ventricular wall, and red arrows indicate microvascular obstruction. RV right ventricular, LGE late gadolinium enhancement, STEMI ST-segment elevation myocardial infarction. (Reprinted with permission from Miszalski-Jamka et al. [82])

Pulmonary Hypertension and Left-Sided Heart Failure

Accurate quantitation of RV volumes and systolic function provides important prognostic information and can be used for risk-stratification in both RV and LV heart failure with reduced and preserved ejection fraction [48–50] and pulmonary artery hypertension [51, 52]. Increased RV to LV volume ratio has been associated with increased all-cause mortality in patients with pulmonary hypertension [51]. Furthermore, CMR RV functional assessment (RV EDV, ESV, and ejection fraction) has contributed to improved medical management of pulmonary hypertension. CMR-derived septal curvature is associated with mortality and can be used to monitor response to pulmonary hypertension therapy [53].

Congenital Heart Disease

The TV and RV are involved in various forms of CHD. CMR is used for both the diagnosis and follow-up of pediatric and adult CHD patients (Table 6.3) [54, 55]. For example, tetralogy of Fallot is the most common form of cyanotic CHD and affects approximately 1 in 3600 live births [56]. With improving care, there are now more adults living with repaired or palliated CHD than their pediatric counterparts, including those with repaired tetralogy of Fallot [57]. CMR is an important tool for

Table 6.3 Right-heart CHD lesions commonly evaluated by CMR in alphabetical order

Lesion	CMR evaluation of right heart
Congenitally corrected transposition of the great arteries	Systemic RV volumes and systolic function Assessment of systemic ventricular fibrosis Quantification of TR If VSD present, useful for quantification of pulmonary versus systemic flow Evaluation of pulmonary stenosis if present Following double switch repair, similar utility as commented below regarding assessment following both arterial and atrial switches
Ebstein anomaly	Functional RV volumes and systolic function Atrialized RV volumes RA volumes Quantification of TR Following repair, evaluation of the TV, RV volumes, and systolic function can be necessary
Secundum atrial septal defect can be useful as an adjunct to echo	RV volume Quantify the shunt volume
Single ventricle with Fontan palliation	Systemic ventricular volumes and systolic function Assessment of systemic ventricular fibrosis Quantification of TR if systemic RV Evaluation of Fontan circuit anatomy and flows to branch pulmonary arteries Quantification of aortopulmonary and venovenous collateral flow
Sinus venosus defect (superior or inferior type)	Assessment of associated partial anomalous pulmonary venous drainage RV volumes Quantification of shunt fraction
Tetralogy of Fallot status post complete repair	Quantification of pulmonary regurgitation and pulmonary stenosis RV volumes and systolic function Assessment of biventricular fibrosis Quantification of associated TR RA volumes Assessment of branch pulmonary artery anatomy and flows

(continued)

Table 6.3 (continued)

Lesion	CMR evaluation of right heart
Transposition of the great arteries status post arterial switch	Quantification of pulmonary regurgitation and pulmonary stenosis RA volumes Quantification of associated TR RV volumes and systolic function Assessment of biventricular fibrosis Assessment of branch pulmonary artery anatomy and flows
Transposition of the great arteries status post atrial switch	Assessment of pulmonary and atrial venous baffles, including quantification of pulmonary versus systemic flow to assess for baffle leak RA volumes Quantification of associated TR RV volumes and systolic function Assessment of branch pulmonary artery anatomy and flows

RA right atrium, *RV* right ventricle, *TR* tricuspid regurgitation, *VSD* ventricular septal defect

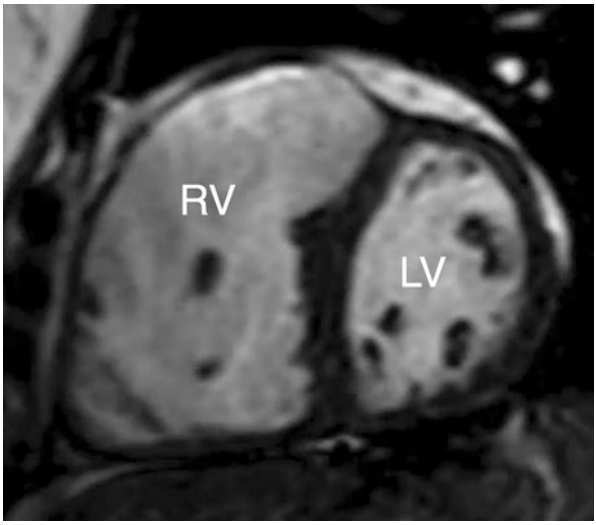

Fig. 6.7 Repaired tetralogy of Fallot with severe right ventricular dilation on cardiovascular magnetic resonance. This short-axis cine at the mid-ventricular level in a patient with repaired TOF demonstrates a severely dilated RV with diastolic flattening of the interventricular septum. TOF tetralogy of Fallot, RV right ventricular, LV left ventricle

follow-up of children and adults with repaired tetralogy of Fallot because the assessment of RV size and systolic function (Fig. 6.7) is important for guiding management and determining the need and timing of pulmonary valve replacement [58, 59]. In fact, both preoperative RV systolic dysfunction and RV-mass-to-volume ratio as determined by CMR relate to occurrence of death or sustained ventricular tachycardia following pulmonary valve replacement [60]. While there is no consensus on criteria for concomitant TV replacement at the time of PVR in repaired TOF [61], intervening on severe TR may be warranted, with CMR often being necessary for more objective quantification. Additionally, CMR affords assessment of the RV outflow tract, including the degree of stenosis and regurgitation, as well as the

branch pulmonary artery anatomy and differential flow. Similar evaluation is often necessary in other forms of repaired CHD leading to RV dilation and systolic dysfunction, such as any patient prone to pulmonary artery or RV-to-pulmonary artery conduit stenosis or regurgitation. Such patients include those with tetralogy of Fallot with pulmonary atresia following complete repair utilizing an RV-to-pulmonary artery conduit, transposition of the great arteries status post arterial switch, or those undergoing a Ross procedure where the native pulmonary root is surgically placed into the aortic position necessitating an RV-to-pulmonary artery conduit [62].

Ebstein's anomaly of the TV involves apical displacement, or in its severe form better described as the rotation of the septal and posterior leaflets of the TV into the RV outflow tract (Fig. 6.8). Both the degree of displacement and extent of development of the posterior and septal leaflet should be interrogated. In fact, a simple measure of the valve rotation angle by CMR prior to the cone surgical reconstruction has been shown to be predictive of unsuccessful repair with subsequent dehiscence [63]. The anterior leaflet retains its normal attachment at the true annulus; however, it is often large and sail-like and can have fenestrations and excessive chordal attachments to the RV free wall limiting its mobility. These are important surgical considerations that need to be meticulously described [64]. While echocardiography plays an important role in delineating the anatomy of the malformed TV, CMR can add value via a more accurate assessment of the degree of tricuspid regurgitation and RV size and function [65]. Additionally, CMR is important in assessing

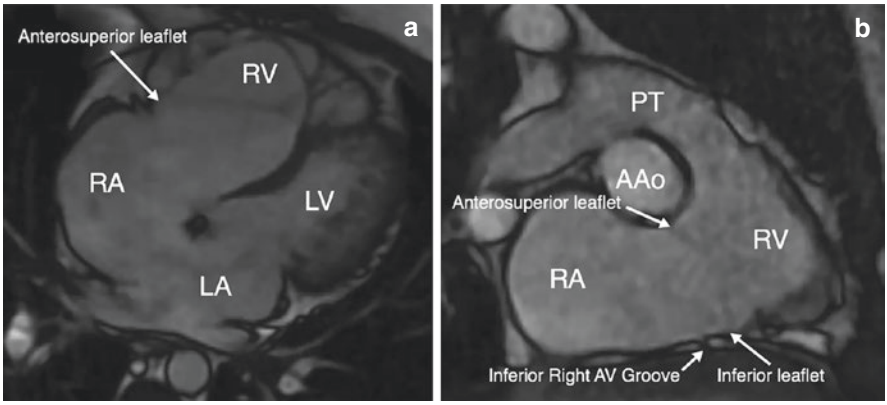

Fig. 6.8 Cardiovascular magnetic resonance imaging in Ebstein anomaly. (**a**) A four-chamber image in a patient with Ebstein's anomaly of the tricuspid valve demonstrates the large and sail-like anterior leaflet retaining its normal hinge with severe displacement and rotation of the septal leaflet toward the right ventricular outflow tract resulting in a large atrialized RV and dilated RA. The LV is heavily trabeculated and meets the criteria for LV noncompaction, a common finding present in up to one-fifth of those with Ebstein's anomaly. (**b**) This RV inflow–outflow cine image again demonstrates the normal hinge point of the anterior leaflet, with mild displacement of the posterior leaflet toward the RV apex. RV right ventricle, RA right atrium, LV left ventricle, AAo ascending aorta, AV atrioventricular, PT pulmonary trunk, LA left atrium

the atrialized RV volume, which relates to exercise capacity [66]. Hemodynamically significant TV abnormalities occur in up to one-third of patients with congenitally corrected transposition of the great arteries, with valvular dysplasia being the most common, followed by Ebstenoid malformation of the TV. In this lesion, the RV is now the systemic ventricle and the TV is exposed to systemic pressures and largely impacted by the interventricular septal position. Competence of the TV now becomes even more important, with the vicious circle of worsening TR and depressed RV systolic function linked to poorer overall outcomes [67]. There are other less common forms of malformation of the TV and RV, which similarly benefit from CMR assessment.

Hypoplastic left heart syndrome (HLHS) is the most common form of CHD with single ventricle physiology [68]. In this disease, patients are born with atretic or severely hypoplastic mitral and aortic valves and undergo serial surgical palliations, ending with the Fontan operation, which connects the systemic veins directly to the branch pulmonary arteries [69]. The RV in this disease is the systemic ventricle, and thus accurate evaluation of ventricular function is crucial as heart failure is a leading cause for mortality in this patient population [70]. CMR provides functional evaluation of the single ventricle, assessment of TR, and evaluation of the Fontan pathway and branch pulmonary arteries, all of which are proven to have a prognostic value in this population [71, 72]. TR can result from structural abnormalities in the TR, and the most common is a small septal leaflet and anterior leaflet prolapse [73]. In addition, frequently encountered abnormalities are valve leaflet dysplasia and leaflet prolapse that alter TV geometry resulting in abnormal coaptation [74–76]. Leaflet tethering can result in restricted leaflet motion, deficient coaptation, and regurgitation. A higher tethering volume has been correlated with increased TR [77]. Tethering can also occur as a consequence of the lateral displacement of the anterior papillary muscle due to the abnormal geometry and dilation of a single RV [73, 77–79]. Abnormal chordae tendinae, including elongation, deficiency, or malattachment, are pathologic findings that result in AVVR. Finally, functional TR occurs in the absence of structural abnormalities of the valve apparatus secondary to ventricular and annular dilation. This results in a stretched annulus and deficient coaptation of valve leaflets. CMR is better suited to evaluate flow and quantify TR in HLHS [80]. Serial CMR exams can assess the progression of ventricular dilation or systolic dysfunction, each of which predisposes to mortality after TR intervention post-Fontan [76]. Other diseases with a systemic RV, including congenitally corrected transposition, as discussed above, and transposition of the great arteries after atrial baffle require serial evaluation of the RV and TR with CMR.

Limitations of MRI

There are limitations to the use of CMR. Implantable devices that are not MRI compatible dictate patient selection. In CHD, the presence of stainless steel or ferromagnetic vascular coils, stents, or occlusion devices may cause imaging artifacts and

limit evaluation by CMR. Quantifying flow by two-dimensional imaging can be especially challenging given the fixed slice location and valvular movement relative to that slice results in through-plane motion. Additionally, image acquisition usually requires an appropriate breath-hold technique over multiple cardiac cycles. Contiguous stacks of cine images along with using a multiplanar approach to imaging the TV are essential to evaluate the anatomy in its entirety. Signal loss can occur when using phase velocity mapping secondary to partial volume averaging or when the size of the voxels (too large) in relation to the size and shape of a jet (narrow) do not match. Structural heterogeneity of the RV in the presence of CHD and arrhythmias can make volumetric analysis both challenging and time-consuming.

References

1. Tretter JT, Sarwark AE, Anderson RH, Spicer DE. Assessment of the anatomical variation to be found in the normal tricuspid valve. Clin Anat (New York, NY). 2016;29(3):399–407.
2. Geva T. Is MRI the preferred method for evaluating right ventricular size and function in patients with congenital heart disease?: MRI is the preferred method for evaluating right ventricular size and function in patients with congenital heart disease. Circ Cardiovasc Imaging. 2014;7(1):190–7.
3. Khalique OK, Cavalcante JL, Shah D, Guta AC, Zhan Y, Piazza N, et al. Multimodality imaging of the tricuspid valve and right heart anatomy. JACC Cardiovasc Imaging. 2019;12(3):516–31.
4. Mooij CF, de Wit CJ, Graham DA, Powell AJ, Geva T. Reproducibility of MRI measurements of right ventricular size and function in patients with normal and dilated ventricles. J Magn Reson Imaging. 2008;28(1):67–73.
5. Mathew RC, Loffler AI, Salerno M. Role of cardiac magnetic resonance imaging in valvular heart disease: diagnosis, assessment, and management. Curr Cardiol Rep. 2018;20(11):119.
6. Hamada-Harimura Y, Seo Y, Ishizu T, Nishi I, Machino-Ohtsuka T, Yamamoto M, et al. Incremental prognostic value of right ventricular strain in patients with acute decompensated heart failure. Circ Cardiovasc Imaging. 2018;11(10):e007249.
7. Gavazzoni M, Badano LP, Vizzardi E, Raddino R, Genovese D, Taramasso M, et al. Prognostic value of right ventricular free wall longitudinal strain in a large cohort of outpatients with left-side heart disease. Eur Heart J Cardiovasc Imaging. 2020;21:1013–21.
8. Gulsin GS, Singh A, McCann GP. Cardiovascular magnetic resonance in the evaluation of heart valve disease. BMC Med Imaging. 2017;17(1):67.
9. Chavhan GB, Babyn PS, Jankharia BG, Cheng HL, Shroff MM. Steady-state MR imaging sequences: physics, classification, and clinical applications. Radiographics. 2008;28(4):1147–60.
10. Maceira AM, Pennell DJ. Chapter 39: Cardiovascular magnetic resonance assessment of right ventricular anatomy and function. In: Manning WJ, Pennell DJ, editors. Cardiovascular magnetic resonance. 3rd ed. Philadelphia: Elsevier; 2019. p. 454–68.e4.
11. Lotz J, Meier C, Leppert A, Galanski M. Cardiovascular flow measurement with phase-contrast MR imaging: basic facts and implementation. Radiographics. 2002;22(3):651–71.
12. Amzulescu MS, De Craene M, Langet H, Pasquet A, Vancraeynest D, Pouleur AC, et al. Myocardial strain imaging: review of general principles, validation, and sources of discrepancies. Eur Heart J Cardiovasc Imaging. 2019;20(6):605–19.
13. Morton G, Schuster A, Jogiya R, Kutty S, Beerbaum P, Nagel E. Inter-study reproducibility of cardiovascular magnetic resonance myocardial feature tracking. J Cardiovasc Magn Reson. 2012;14(1):43.

14. Taylor RJ, Moody WE, Umar F, Edwards NC, Taylor TJ, Stegemann B, et al. Myocardial strain measurement with feature-tracking cardiovascular magnetic resonance: normal values. Eur Heart J Cardiovasc Imaging. 2015;16(8):871–81.
15. Truong VT, Safdar KS, Kalra DK, Gao X, Ambach S, Taylor MD, et al. Cardiac magnetic resonance tissue tracking in right ventricle: feasibility and normal values. Magn Reson Imaging. 2017;38:189–95.
16. van Lammeren GW, Catanzariti LM, Peelen LM, de Vries JP, de Kleijn DP, Moll FL, et al. Clinical prediction rule to estimate the absolute 3-year risk of major cardiovascular events after carotid endarterectomy. Stroke. 2012;43(5):1273–8.
17. Sarikouch S, Koerperich H, Boethig D, Peters B, Lotz J, Gutberlet M, et al. Reference values for atrial size and function in children and young adults by cardiac MR: a study of the German competence network congenital heart defects. J Magn Reson Imaging. 2011;33(5):1028–39.
18. Lamy J, Soulat G, Evin M, Huber A, de Cesare A, Giron A, et al. Scan-rescan reproducibility of ventricular and atrial MRI feature tracking strain. Comput Biol Med. 2018;92:197–203.
19. Pontecorboli G, Figueras IVRM, Carlosena A, Benito E, Prat-Gonzales S, Padeletti L, et al. Use of delayed-enhancement magnetic resonance imaging for fibrosis detection in the atria: a review. Europace. 2017;19(2):180–9.
20. Mori S, Tretter JT, Spicer DE, Bolender DL, Anderson RH. What is the real cardiac anatomy? Clin Anat (New York, NY). 2019;32(3):288–309.
21. Sutton JP 3rd, Ho SY, Vogel M, Anderson RH. Is the morphologically right atrioventricular valve tricuspid? J Heart Valve Dis. 1995;4(6):571–5.
22. Fukuda S, Saracino G, Matsumura Y, Daimon M, Tran H, Greenberg NL, et al. Three-dimensional geometry of the tricuspid annulus in healthy subjects and in patients with functional tricuspid regurgitation: a real-time, 3-dimensional echocardiographic study. Circulation. 2006;114(1 Suppl):I492–8.
23. Anwar AM, Soliman OI, Nemes A, van Geuns RJ, Geleijnse ML, Ten Cate FJ. Value of assessment of tricuspid annulus: real-time three-dimensional echocardiography and magnetic resonance imaging. Int J Cardiovasc Imaging. 2007;23(6):701–5.
24. Maffessanti F, Gripari P, Pontone G, Andreini D, Bertella E, Mushtaq S, et al. Three-dimensional dynamic assessment of tricuspid and mitral annuli using cardiovascular magnetic resonance. Eur Heart J Cardiovasc Imaging. 2013;14(10):986–95.
25. Naoum C, Blanke P, Cavalcante JL, Leipsic J. Cardiac computed tomography and magnetic resonance imaging in the evaluation of mitral and tricuspid valve disease: implications for transcatheter interventions. Circ Cardiovasc Imaging. 2017;10(3):e005331.
26. Anderson RH, Mohun TJ, Moorman AF. What is a ventricle? Cardiol Young. 2011;21(Suppl 2):14–22.
27. Anderson RH, Tretter JT, Spicer DE, Mori S. The fate of the outflow tract septal complex in relation to the classification of ventricular septal defects. J Cardiovasc Dev Dis. 2019;6(1):9.
28. Sanz J, Sanchez-Quintana D, Bossone E, Bogaard HJ, Naeije R. Anatomy, function, and dysfunction of the right ventricle: JACC state-of-the-art review. J Am Coll Cardiol. 2019;73(12):1463–82.
29. Redington AN, Gray HH, Hodson ME, Rigby ML, Oldershaw PJ. Characterisation of the normal right ventricular pressure-volume relation by biplane angiography and simultaneous micromanometer pressure measurements. Br Heart J. 1988;59(1):23–30.
30. Bisbal F, Baranchuk A, Braunwald E, Bayes de Luna A, Bayes-Genis A. Atrial failure as a clinical entity: JACC review topic of the week. J Am Coll Cardiol. 2020;75(2):222–32.
31. Alenezi F, Mandawat A, Il'Giovine ZJ, Shaw LK, Siddiqui I, Tapson VF, et al. Clinical utility and prognostic value of right atrial function in pulmonary hypertension. Circ Cardiovasc Imaging. 2018;11(11):e006984.
32. Vitarelli A, Mangieri E, Gaudio C, Tanzilli G, Miraldi F, Capotosto L. Right atrial function by speckle tracking echocardiography in atrial septal defect: prediction of atrial fibrillation. Clin Cardiol. 2018;41(10):1341–7.

33. Meng X, Li Y, Li H, Wang Y, Zhu W, Lu X. Right atrial function in patients with pulmonary hypertension: a study with two-dimensional speckle-tracking echocardiography. Int J Cardiol. 2018;255:200–5.
34. Sallach JA, Tang WH, Borowski AG, Tong W, Porter T, Martin MG, et al. Right atrial volume index in chronic systolic heart failure and prognosis. JACC Cardiovasc Imaging. 2009;2(5):527–34.
35. Maceira AM, Cosin-Sales J, Prasad SK, Pennell DJ. Characterization of left and right atrial function in healthy volunteers by cardiovascular magnetic resonance. J Cardiovasc Magn Reson. 2016;18(1):64.
36. Kutty S, Shang Q, Joseph N, Kowallick JT, Schuster A, Steinmetz M, et al. Abnormal right atrial performance in repaired tetralogy of Fallot: a CMR feature tracking analysis. Int J Cardiol. 2017;248:136–42.
37. Jun H, Park EA, Bahn YE, Lee W, Kim HK, Chung JW. Quantification of tricuspid regurgitation using two-dimensional velocity encoding cine: optimal plane and reproducibility. Int J Cardiovasc Imaging. 2015;31(Suppl 2):233–40.
38. Baumgartner H, Falk V, Bax JJ, De Bonis M, Hamm C, Holm PJ, et al. 2017 ESC/EACTS guidelines for the management of valvular heart disease. Eur Heart J. 2017;38(36):2739–91.
39. Nishimura RA, Otto CM, Bonow RO, Carabello BA, Erwin JP 3rd, Guyton RA, et al. 2014 AHA/ACC guideline for the management of patients with valvular heart disease: executive summary: a report of the American College of Cardiology/American Heart Association Task Force on practice guidelines. Circulation. 2014;129(23):2440–92.
40. Nickenig G, Weber M, Schueler R, Hausleiter J, Nabauer M, von Bardeleben RS, et al. 6-month outcomes of tricuspid valve reconstruction for patients with severe tricuspid regurgitation. J Am Coll Cardiol. 2019;73(15):1905–15.
41. Kim HK, Kim YJ, Park EA, Bae JS, Lee W, Kim KH, et al. Assessment of haemodynamic effects of surgical correction for severe functional tricuspid regurgitation: cardiac magnetic resonance imaging study. Eur Heart J. 2010;31(12):1520–8.
42. Shah S, Jenkins T, Markowitz A, Gilkeson R, Rajiah P. Multimodal imaging of the tricuspid valve: normal appearance and pathological entities. Insights Imaging. 2016;7(5):649–67.
43. Saremi F, Hassani C, Millan-Nunez V, Sanchez-Quintana D. Imaging evaluation of tricuspid valve: analysis of morphology and function with CT and MRI. AJR Am J Roentgenol. 2015;204(5):W531–42.
44. Andersen HR, Falk E, Nielsen D. Right ventricular infarction: frequency, size and topography in coronary heart disease: a prospective study comprising 107 consecutive autopsies from a coronary care unit. Am J Cardiol. 1987;10(6):1223–32.
45. Isner JM, Roberts WC. Right ventricular infarction complicating left ventricular infarction secondary to coronary heart disease. Frequency, location, associated findings and significance from analysis of 236 necropsy patients with acute or healed myocardial infarction. Am J Cardiol. 1978;42(6):885–94.
46. Shah PK, Maddahi J, Berman DS, Pichler M, Swan HJ. Scintigraphically detected predominant right ventricular dysfunction in acute myocardial infarction: clinical and hemodynamic correlates and implications for therapy and prognosis. J Am Coll Cardiol. 1985;6(6):1264–72.
47. Inohara T, Kohsaka S, Fukuda K, Menon V. The challenges in the management of right ventricular infarction. Eur Heart J Acute Cardiovasc Care. 2013;2(3):226–34.
48. Aschauer S, Tufaro C, Kammerlander A, Bachmann AF, Bondermann D, Mascherbauer J. Prevalence and prognostic significance of right ventricular systolic dysfunction in heart failure with preserved ejection fraction. Insights from a cardiac magnetic resonance imaging study. J Cardiovasc Magn Reson. 2015;17(S1):O33.
49. Bosch L, Lam CSP, Gong L, Chan SP, Sim D, Yeo D, et al. Right ventricular dysfunction in left-sided heart failure with preserved versus reduced ejection fraction. Eur J Heart Failure. 2017;19(12):1664–71.

50. Meyer P, Filippatos GS, Ahmed MI, Iskandrian AE, Bittner V, Perry GJ, et al. Effects of right ventricular ejection fraction on outcomes in chronic systolic heart failure. Circulation. 2010;121(2):252–8.
51. Altmayer SPL, Han QJ, Addetia K, Patel AR, Forfia PR, Han Y. Using all-cause mortality to define severe RV dilation with RV/LV volume ratio. Sci Rep. 2018;8(1):7200.
52. Peacock AJ, Crawley S, McLure L, Blyth KG, Vizza CD, Poscia R, et al. Changes in right ventricular function measured by cardiac magnetic resonance imaging in patients receiving pulmonary arterial hypertension-targeted therapy: the EURO-MR study. Circ Cardiovasc Imaging. 2014;7(1):107–14.
53. Pandya B, Quail MA, Steeden JA, McKee A, Odille F, Taylor AM, et al. Real-time magnetic resonance assessment of septal curvature accurately tracks acute hemodynamic changes in pediatric pulmonary hypertension. Circ Cardiovasc Imaging. 2014;7(4):706–13.
54. Fratz S, Chung T, Greil GF, Samyn MM, Taylor AM, Valsangiacomo Buechel ER, et al. Guidelines and protocols for cardiovascular magnetic resonance in children and adults with congenital heart disease: SCMR expert consensus group on congenital heart disease. J Cardiovasc Magn Reson. 2013;15:51.
55. Burchill LJ, Huang J, Tretter JT, Khan AM, Crean AM, Veldtman GR, et al. Noninvasive imaging in adult congenital heart disease. Circ Res. 2017;120(6):995–1014.
56. Hoffman JI, Kaplan S. The incidence of congenital heart disease. J Am Coll Cardiol. 2002;39(12):1890–900.
57. Marelli AJ, Ionescu-Ittu R, Mackie AS, Guo L, Dendukuri N, Kaouache M. Lifetime prevalence of congenital heart disease in the general population from 2000 to 2010. Circulation. 2014;130(9):749–56.
58. Geva T. Repaired tetralogy of Fallot: the roles of cardiovascular magnetic resonance in evaluating pathophysiology and for pulmonary valve replacement decision support. J Cardiovasc Magn Reson. 2011;13:9.
59. Tretter JT, Friedberg MK, Wald RM, McElhinney DB. Defining and refining indications for transcatheter pulmonary valve replacement in patients with repaired tetralogy of Fallot: contributions from anatomical and functional imaging. Int J Cardiol. 2016;221:916–25.
60. Geva T, Mulder B, Gauvreau K, Babu-Narayan SV, Wald RM, Hickey K, et al. Preoperative predictors of death and sustained ventricular tachycardia after pulmonary valve replacement in patients with repaired tetralogy of fallot enrolled in the INDICATOR Cohort. Circulation. 2018;138(19):2106–15.
61. Tretter JT, Redington AN. To repair or not to repair: who should undergo tricuspid valve repair at the time of pulmonary valve replacement in previously repaired tetralogy of Fallot. J Thorac Cardiovasc Surg. 2017;154(1):224–5.
62. Deshaies C, Trottier H, Khairy P, Al-Aklabi M, Beauchesne L, Bernier PL, et al. Tricuspid intervention following pulmonary valve replacement in adults with congenital heart disease. J Am Coll Cardiol. 2020;75(9):1033–43.
63. Hughes ML, Bonello B, Choudhary P, Marek J, Tsang V. A simple measure of the extent of Ebstein valve rotation with cardiovascular magnetic resonance gives a practical guide to feasibility of surgical cone reconstruction. J Cardiovasc Magn Reson. 2019;21(1):34.
64. Tretter JT, Anderson RH. Ebstein's or Prescher's anomaly? Eur Heart J. 2018;39(12):972–3.
65. Kuhn A, Meierhofer C, Rutz T, Rondak IC, Rohlig C, Schreiber C, et al. Non-volumetric echocardiographic indices and qualitative assessment of right ventricular systolic function in Ebstein's anomaly: comparison with CMR-derived ejection fraction in 49 patients. Eur Heart J Cardiovasc Imaging. 2016;17(8):930–5.
66. Tobler D, Yalonetsky S, Crean AM, Granton JT, Burchill L, Silversides CK, et al. Right heart characteristics and exercise parameters in adults with Ebstein anomaly: new perspectives from cardiac magnetic resonance imaging studies. Int J Cardiol. 2013;165(1):146–50.
67. Whiteside W, Tretter JT, Aboulhosn J, Aldoss O, Armstrong AK, Bocks ML, et al. Acute and midterm outcomes of transcatheter pulmonary valve replacement for treatment of dysfunctional left ventricular outflow tract conduits in patients with aortopulmonary transposition and a systemic right ventricle. Circ Cardiovasc Interv. 2017;10(9):e004730.

68. Alsaied T, Tseng S, King E, Hahn E, Divanovic A, Habli M, et al. Effect of fetal hemodynamics on growth in fetuses with single ventricle or transposition of the great arteries. Ultrasound Obstet Gynecol. 2018;52(4):479–87.
69. Alsaied T, Bokma JP, Engel ME, Kuijpers JM, Hanke SP, Zuhlke L, et al. Predicting long-term mortality after Fontan procedures: a risk score based on 6707 patients from 28 studies. Congenit Heart Dis. 2017;12(4):393–8.
70. Alsaied T, Bokma JP, Engel ME, Kuijpers JM, Hanke SP, Zuhlke L, et al. Factors associated with long-term mortality after Fontan procedures: a systematic review. Heart. 2017;103(2):104–10.
71. Alsaied T, Sleeper LA, Masci M, Ghelani SJ, Azcue N, Geva T, et al. Maldistribution of pulmonary blood flow in patients after the Fontan operation is associated with worse exercise capacity. J Cardiovasc Magn Reson. 2018;20(1):85.
72. Alsaied T, van der Ven JPG, Juggan S, Sleeper LA, Azcue N, Kroft LJ, et al. Relation of Fontan Baffle stroke volume to Fontan failure and lower exercise capacity in patients with an Atriopulmonary Fontan. Am J Cardiol. 2019;124(1):151–7.
73. Takahashi K, Inage A, Rebeyka IM, Ross DB, Thompson RB, Mackie AS, et al. Real-time 3-dimensional echocardiography provides new insight into mechanisms of tricuspid valve regurgitation in patients with hypoplastic left heart syndrome. Circulation. 2009;120(12):1091–8.
74. Tsang VT, Raja SG. Tricuspid valve repair in single ventricle: timing and techniques. Semin Thorac Cardiovasc Surg Pediatr Card Surg Annu. 2012;15(1):61–8.
75. Ohye RG, Gomez CA, Goldberg CS, Graves HL, Devaney EJ, Bove EL. Tricuspid valve repair in hypoplastic left heart syndrome. J Thoracic Cardiovasc Surg. 2004;127(2):465–72.
76. Honjo O, Atlin CR, Mertens L, Al-Radi OO, Redington AN, Caldarone CA, et al. Atrioventricular valve repair in patients with functional single-ventricle physiology: impact of ventricular and valve function and morphology on survival and reintervention. J Thoracic Cardiovasc Surg. 2011;142(2):326–35 e2.
77. Kutty S, Colen T, Thompson RB, Tham E, Li L, Vijarnsorn C, et al. Tricuspid regurgitation in hypoplastic left heart syndrome: mechanistic insights from 3-dimensional echocardiography and relationship with outcomes. Circ Cardiovasc Imaging. 2014;7(5):765–72.
78. Nguyen AV, Lasso A, Nam HH, Faerber J, Aly AH, Pouch AM, et al. Dynamic three-dimensional geometry of the tricuspid valve annulus in hypoplastic left heart syndrome with a fontan circulation. J Am Soc Echocardiogr. 2019;32(5):655–66 e13.
79. Nii M, Guerra V, Roman KS, Macgowan CK, Smallhorn JF. Three-dimensional tricuspid annular function provides insight into the mechanisms of tricuspid valve regurgitation in classic hypoplastic left heart syndrome. J Am Soc Echocardiogr. 2006;19(4):391–402.
80. Hauser JA, Taylor AM, Pandya B. How to image the adult patient with Fontan circulation. Circ Cardiovasc Imaging. 2017;10(5):e004273.
81. Petersen SE, Aung N, Sanghvi MM, Zemrak F, Fung K, Paiva JM, et al. Reference ranges for cardiac structure and function using cardiovascular magnetic resonance (CMR) in Caucasians from the UK biobank population cohort. J Cardiovasc Magn Reson. 2017;19(1):18.
82. Miszalski-Jamka T, Klimeczek P, Tomala M, Krupinski M, Zawadowski G, Noelting J, et al. Extent of RV dysfunction and myocardial infarction assessed by CMR are independent outcome predictors early after STEMI treated with primary angioplasty. J Am Coll Cardiol Img. 2010;3(12):1237–46.